

Sparse travel time tomography with adaptive dictionaries

Michael Bianco, *Student Member, IEEE*, Peter Gerstoft, *Member, IEEE*,

Abstract—We develop a 2D travel time tomography method which regularizes the inversion by modeling groups of slowness pixels from discrete slowness maps, called patches, as sparse linear combinations of atoms from a dictionary. We further propose to learn optimal slowness dictionaries using dictionary learning, in parallel with the inversion. This patch regularization, which we call the local model, is integrated into the overall slowness map, called the global model. Where the local model considers small-scale variations using a sparsity constraint, the global model considers larger-scale features which are constrained using ℓ_2 -norm regularization. This local-global modeling strategy with dictionary learning has been successful for image restoration tasks such as denoising and inpainting, where diverse image content is recovered from noisy or incomplete measurements. We use this strategy in our locally-sparse travel time tomography (LST) approach to model simultaneously smooth and discontinuous slowness features. This is in contrast to conventional tomography methods, which constrain models to be exclusively smooth or discontinuous. We develop a *maximum a posteriori* formulation for LST and exploit the sparsity of slowness patches using dictionary learning. We demonstrate the LST approach on densely, but irregularly sampled synthetic slowness maps.

Index Terms—Dictionary learning, machine learning, inverse problems, geophysics, seismics, sparse modeling

I. INTRODUCTION

Travel time tomography methods estimate Earth slowness structure, which contains smooth and discontinuous features at multiple spatial scales, from travel times of seismic waves between recording stations. The estimation of slowness (inverse of speed) models from travel times is often formulated as a discrete linear inverse problem, where the perturbations in travel time relative to a reference are used to infer the unknown structure [1], [2]. Such problems are ill-posed, with irregular ray coverage of environments, and require regularization to obtain physically plausible solutions.

We propose a 2D travel time tomography method which regularizes the inversion by assuming small groups of slowness pixels from a discrete slowness map, called patches, are well modeled with sparse linear combinations of atoms from a dictionary. In this sparse model [3], [4], the atoms represent elemental slowness patches and can be generic dictionaries, e.g. wavelets, or adapted specifically to the data by dictionary learning [5], [6]. This patch regularization, which we call the local model, is integrated into the overall slowness map, called the global model. Whereas the local model considers small-scale variations using a sparsity constraint, the global model considers larger-scale features which are constrained using ℓ_2 -norm regularization.

This local-global modeling strategy with dictionary learning has been successful for image denoising [3], [7], [8] and inpainting [9], where diverse image content is recovered from noisy or incomplete measurements. We use this strategy to better recover true slowness fields from travel time tomography by simultaneously modeling smooth and discontinuous slowness features. This gives an improvement over conventional methods with global damping and smoothness regularization [2], [10] and pixel level regularization e.g. total variation regularization [11], [12] which regularize tomography by restrict the slowness models to be specifically smooth or discontinuous. Relative to existing tomography methods based on wavelets [13], [14] and sparse dictionaries [15], [16], our formulation of the tomography problem permits the adaptation of the sparse dictionaries to travel time data and ray sampling by dictionary learning techniques, for which many methods exist [3], [5], [6], [8], [17]. It has been shown that sparse reconstruction performance is often improved using adaptive dictionaries, which are represent well specific data, over generic dictionaries which achieve acceptable performance for many tasks [4].

Sparse modeling assumes signals can be reconstructed to acceptable accuracy using few or *sparse* vectors, called *atoms*, from a potentially large set or *dictionary* of atoms. The parsimony of sparse representations [4] often provides improved inverse problem regularization over for example traditional ℓ_2 -norm model damping [2]. A sparse approach to seismic deconvolution was proposed early in [18], and this philosophy has since become ubiquitous in signal processing for image and video denoising [3], [7], [8] and inpainting [9], and medical imaging [19], [20], to name a few examples. Recent works in acoustics and seismics have utilized sparse modeling, e.g. beamforming [21], [22], matched field processing [23], and inversion for ocean acoustic properties [24]–[27]. Dictionary learning based methods have been used to denoise seismic traces [28], [29] and ocean acoustic recordings [30], regularize full waveform inversion [31], and regularize ocean sound speed profile inversion [24], [25].

We develop a sparse and adaptive 2D travel time tomography method, which we refer to as locally-sparse travel time tomography (LST). This approach is similar to works in image denoising [7] and CS magnetic resonance imaging (MRI) [20]. We develop a *maximum a posteriori* (MAP) formulation to the problem and use the iterative thresholding and signed K-means (ITKM) [6] dictionary learning algorithm to design adaptive dictionaries. This improves slowness models over generic dictionaries. We demonstrate the performance of LST for 2D surface wave tomography with synthetic slowness maps and travel time data. The results are compared with

conventional tomography.

II. OVERVIEW OF LST

Given travel time perturbations $\mathbf{t} \in \mathbb{R}^M$ from M ray paths through a discrete slowness map, and tomography matrix $\mathbf{A} \in \mathbb{R}^{M \times N}$, which gives the discrete path lengths of M rays through N pixels, see Fig. 1(a), LST estimates the *sparse slowness* \mathbf{s}_s . We first estimate the *global slowness* \mathbf{s}_g , which is determined by \mathbf{t} . Then, \mathbf{s}_g is used to obtain the *patch slowness* $\mathbf{D}\mathbf{x}_i$ for patch i , where $\mathbf{D} \in \mathbb{R}^{n \times Q}$ is a dictionary of Q atoms, and $\mathbf{x}_i \in \mathbb{R}^n$ is the sparse coefficients with n the number of pixels in a patch. Finally, slownesses $\{\mathbf{D}\hat{\mathbf{x}}_i \forall i\}$ are averaged with \mathbf{s}_g to obtain \mathbf{s}_s per (18).

A. Global slowness and travel time

We discretize a 2D slowness map as a $W_1 \times W_2$ pixel image, shown in Fig. 1(a), where each pixel has constant slowness. The slowness pixels are represented by the vector $\mathbf{s}' = \mathbf{s}_g + \mathbf{s}_0 \in \mathbb{R}^N$, where \mathbf{s}_0 is reference slownesses and \mathbf{s}_g is perturbations from the reference, with $N = W_1 W_2$. We assume travel time observations $\mathbf{t}' = \mathbf{t} + \mathbf{t}_0$ from M straight ray paths, where \mathbf{t}_0 and \mathbf{t} are the reference travel time and perturbations. Since \mathbf{s}_0 and $\mathbf{t}_0 = \mathbf{A}\mathbf{s}_0$ are known, we estimate the perturbations

$$\mathbf{t} = \mathbf{A}\mathbf{s}_g + \boldsymbol{\epsilon}, \quad (1)$$

where $\boldsymbol{\epsilon} \in \mathbb{R}^M$ is Gaussian noise $\mathcal{N}(\mathbf{0}, \sigma_\epsilon^2 \mathbf{I})$, with mean $\mathbf{0}$ and covariance $\sigma_\epsilon^2 \mathbf{I}$. We call (1) the *global model*, as it captures the large-scale features that span the discrete map and generates \mathbf{t} . We assume dense ray coverage, and do not explicitly account for varying coverage density (see Sec. III).

B. Local sparse model

Each patch is a $\sqrt{n} \times \sqrt{n}$ group of pixels from \mathbf{s}_s , see Fig. 1(a). The patches are selected from \mathbf{s}_s by the binary matrix $\mathbf{R}_i \in \{0, 1\}^{n \times N}$. Hence the slownesses in patch i are $\mathbf{R}_i \mathbf{s}_s$. Each patch is indexed by the row w_1 and column w_2 of its top-left pixel in the 2D image as $(w_{1,i}, w_{2,i})$. We consider all overlapping patches, with $w_{1,i}$ and $w_{2,i}$ differing from their neighbor by ± 1 (*stride* of one). Thus, for a $W_1 \times W_2$ pixel image, the number of patches is $I = (W_1 - \sqrt{n} + 1)(W_2 - \sqrt{n} + 1)$.

$\mathbf{R}_i \mathbf{s}_s$ is approximated by sparse linear combinations atoms from \mathbf{D} . The coefficients are estimated by

$$\hat{\mathbf{x}}_i = \arg \min_{\mathbf{x}_i} \|\mathbf{R}_i \mathbf{s}_s - \mathbf{D}\mathbf{x}_i\|_2^2 \text{ subject to } \|\mathbf{x}_i\|_0 = T, \quad (2)$$

where $\hat{\mathbf{x}}_i \in \mathbb{R}^n$ is the coefficient estimates and T is the number of non-zero coefficients. The ℓ_0 pseudo-norm penalizes the number of non-zero coefficients [3]. $\mathbf{D}\hat{\mathbf{x}}_i$ is the patch slowness. We call (2) the *local model*, as it captures the smaller scale, localized features contained by patches.

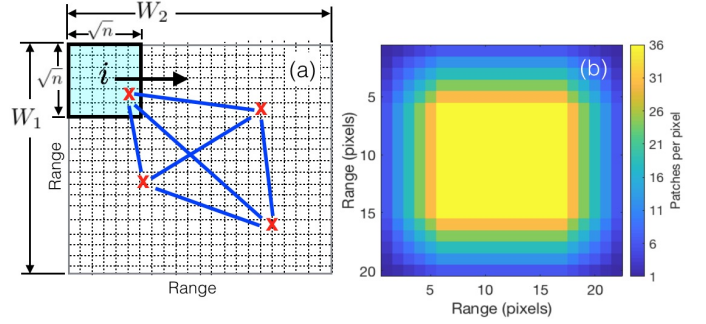


Fig. 1. 2D slowness image corresponds to (a) slowness map divided into pixels (dashed boxes). The square image patch i contains n pixels. W_1 and W_2 are the vertical and horizontal dimensions of the image (in pixels), which give I unique patches. Sensors are shown as red x 's and the ray paths between the sensors are shown as blue lines. The number of blocks that contain the pixels is illustrated in (b) for the configuration in (a) with $W_1 = 20$, $W_2 = 22$, and $n = 36$.

C. Dictionaries

The atoms in \mathbf{D} are considered “elemental patches”, where only a small number of atoms from $Q \ll I$ are necessary to adequately approximate $\mathbf{R}_i \mathbf{s}_s$. Atoms can be generic functions, e.g. wavelets or the discrete cosine transform (DCT), or learned from the data (see Sec. III-B). An example of DCT atoms are shown in Fig. 2. Adaptive dictionaries, which are designed from the data using dictionary learning algorithms, often achieve greater reconstruction accuracy over generic dictionaries. Examples of dictionaries learned from synthetic travel time data (from slowness maps in Fig. 3) are shown in Fig. 4. Relative to generic dictionaries, learned dictionaries can represent the smooth and discontinuous seismic features we are likely to encounter in real inversion scenarios.

D. Outline of inversion approach

1) *Relating local and global models*: To combine the global and local models, we formulate the inversion as two corresponding subproblems [7]. The global image structure is obtained solving (1) using least squares with ℓ_2 -norm regularization. The local structure is obtained by solving for the patches by (2), and averaging the patches. In Sec. III, we derive the MAP formulation of LST.

Global ℓ_2 -norm regularization has been used in conjunction with total variation regularization in seismic tomography [11], which was an extension of [32]. Our result combines a global ℓ_2 -norm constraint with local regularization of patches, following [3].

2) *Dictionary learning*: Both generic and learned dictionaries are used in the inversion. We demonstrate that the adaptation of \mathbf{D} to seismic data by dictionary learning further improves the model fit of LST. Dictionary learning is introduced into the MAP solution during the sparse solution stage to improve the dictionary entries and coefficient estimates. We use the Iterative Thresholding and K-means (ITKM) dictionary learning algorithm [6] to learn the dictionary. For details see Appendix.

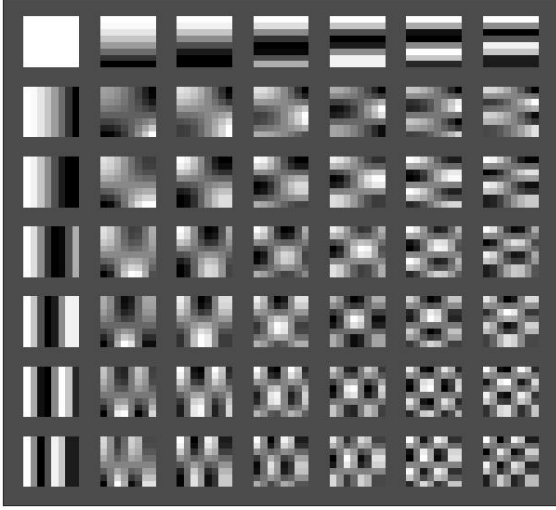


Fig. 2. Discrete cosine transform (DCT) dictionary atoms. The $Q = 49$ atoms (ordered in a 7×7 grid) each contain $n = 8 \times 8 = 64$ pixels. Atom values stretched to full grayscale range for display.

E. Advantages

Improved inversion performance over conventional tomography is obtained under the hypothesis that the seismic image patches can be represented as sparse linear combinations a finite number of elemental patches, or patterns. Such patterns are the atoms in the dictionary \mathbf{D} . This hypothesis follows numerous works in image processing and neuroscience communities, for example [3], [8], [17], [33], which have shown that patches of diverse image content are well approximated with a sparse linear combinations of atoms. This property has been exploited for signal denoising and inpainting [3], [8] and classification [9], [34].

As previously mentioned, sparse dictionaries are capable of modeling diverse image content. Further, sparse dictionaries possess the *shift-invariance* property, which allows sparse models to estimate features such as edges regardless of where they are located in an image [3]. LST enables finer resolution as permitted by the atoms in the dictionary and can exploit shift invariance. Slowness features in Fig. 3(a–b) are shifted such that only small cells of constant slowness may be used with conventional tomography (which necessitates damping, Sec. III-C) to illustrate this effect.

III. DERIVATION OF LST MAP OBJECTIVE

Starting with Bayes' rule, we here derive the LST MAP objective for the slowness \mathbf{s}_s , incorporating both the patch-sparsity prior and global constraints. For the derivation of the MAP objective, we assume the dictionary \mathbf{D} and sensing matrix \mathbf{A} known. In Sec. III-B, dictionary learning is included in the algorithm.

The posterior density is formulated as

$$\begin{aligned} p(\mathbf{s}_g, \mathbf{s}_s, \mathbf{X} | \mathbf{t}) &\propto p(\mathbf{t} | \mathbf{s}_g, \mathbf{s}_s, \mathbf{X}) p(\mathbf{s}_g, \mathbf{s}_s, \mathbf{X}) \\ &\propto p(\mathbf{t} | \mathbf{s}_g, \mathbf{s}_s, \mathbf{X}) p(\mathbf{s}_g | \mathbf{s}_s, \mathbf{X}) p(\mathbf{s}_s, \mathbf{X}) \\ &\propto p(\mathbf{t} | \mathbf{s}_g, \mathbf{s}_s, \mathbf{X}) p(\mathbf{s}_g | \mathbf{s}_s, \mathbf{X}) p(\mathbf{s}_s | \mathbf{X}) p(\mathbf{X}), \end{aligned} \quad (3)$$

where $\mathbf{X} = [\mathbf{x}_1, \dots, \mathbf{x}_I] \in \mathbb{R}^{Q \times I}$ are the coefficients describing all patches I . If \mathbf{s}_g (\mathbf{s}_s) is known, so is \mathbf{t} (\mathbf{s}_g), whereby

$$p(\mathbf{s}_g, \mathbf{s}_s, \mathbf{X} | \mathbf{t}) \propto p(\mathbf{t} | \mathbf{s}_g) p(\mathbf{s}_g | \mathbf{s}_s) p(\mathbf{s}_s | \mathbf{X}) p(\mathbf{X}), \quad (4)$$

First considering the global problem, we approximate $p(\mathbf{t} | \mathbf{s}_g)$ and $p(\mathbf{s}_g | \mathbf{s}_s)$ as

$$\begin{aligned} p(\mathbf{t} | \mathbf{s}_g) &= \mathcal{N}(\mathbf{A}\mathbf{s}_g, \mathbf{\Sigma}_\epsilon) \\ p(\mathbf{s}_g | \mathbf{s}_s) &= \mathcal{N}(\mathbf{s}_g, \mathbf{\Sigma}_g), \end{aligned} \quad (5)$$

where $\mathbf{\Sigma}_\epsilon \in \mathbb{R}^{K \times K}$ is the covariance of the travel time error and $\mathbf{\Sigma}_g \in \mathbb{R}^{N \times N}$ is the covariance of \mathbf{s}_g . Taking the logarithm of (5), we obtain

$$\begin{aligned} \ln p(\mathbf{t} | \mathbf{s}_g) &\propto -\frac{1}{2}(\mathbf{t} - \mathbf{A}\mathbf{s}_g)^T \mathbf{\Sigma}_\epsilon^{-1} (\mathbf{t} - \mathbf{A}\mathbf{s}_g), \\ \ln p(\mathbf{s}_g | \mathbf{s}_s) &\propto -\frac{1}{2}(\mathbf{s}_g - \mathbf{s}_s)^T \mathbf{\Sigma}_g^{-1} (\mathbf{s}_g - \mathbf{s}_s). \end{aligned} \quad (6)$$

Now considering the local problem, the slowness estimates for patches $i = 1 \dots I$ are considered statistically independent, and the patch likelihood is

$$p(\mathbf{s}_s | \mathbf{X}) = \prod_i p(\mathbf{R}_i \mathbf{s}_s | \mathbf{x}_i) = \prod_i \mathcal{N}(\mathbf{D}\mathbf{x}_i, \mathbf{\Sigma}_{p,i}), \quad (7)$$

where $\mathbf{\Sigma}_{p,i} \in \mathbb{R}^{n \times n}$ is the covariance of the patch slownesses. Taking the logarithm of (7),

$$\ln p(\mathbf{s}_s | \mathbf{X}) \propto -\frac{1}{2} \sum_i (\mathbf{D}\mathbf{x}_i - \mathbf{R}_i \mathbf{s}_s)^T \mathbf{\Sigma}_{p,i}^{-1} (\mathbf{D}\mathbf{x}_i - \mathbf{R}_i \mathbf{s}_s). \quad (8)$$

Assuming the coefficients \mathbf{x}_i describing patch $\mathbf{R}_i \mathbf{s}_s$ are independent,

$$\ln p(\mathbf{X}) = \sum_i \ln p(\mathbf{x}_i). \quad (9)$$

From (4), and (6), (8), and (9),

$$\begin{aligned} \ln p(\mathbf{s}_g, \mathbf{s}_s, \mathbf{X} | \mathbf{t}) &\propto \ln \{ p(\mathbf{t} | \mathbf{s}_g) p(\mathbf{s}_g | \mathbf{s}_s) p(\mathbf{s}_s | \mathbf{X}) p(\mathbf{X}) \} \\ &\propto -(\mathbf{t} - \mathbf{A}\mathbf{s}_g)^T \mathbf{\Sigma}_\epsilon^{-1} (\mathbf{t} - \mathbf{A}\mathbf{s}_g) - (\mathbf{s}_g - \mathbf{s}_s)^T \mathbf{\Sigma}_g^{-1} (\mathbf{s}_g - \mathbf{s}_s) \\ &\quad - \sum_i \left\{ (\mathbf{D}\mathbf{x}_i - \mathbf{R}_i \mathbf{s}_s)^T \mathbf{\Sigma}_{p,i}^{-1} (\mathbf{D}\mathbf{x}_i - \mathbf{R}_i \mathbf{s}_s) + 2 \ln p(\mathbf{x}_i) \right\}. \end{aligned} \quad (10)$$

Assuming the coefficients \mathbf{x}_i sparse, we approximate $\ln p(\mathbf{x}_i)$ with the ℓ_0 pseudo-norm $\|\mathbf{x}_i\|_0$. We further assume the number of non-zero coefficients T is the same for every patch. Hence the MAP solution is

$$\begin{aligned} \max \{ \ln p(\mathbf{s}_g, \mathbf{s}_s, \mathbf{X} | \mathbf{t}) \} &= \min \{ -\ln p(\mathbf{s}_g, \mathbf{s}_s, \mathbf{X} | \mathbf{t}) \} \\ &\propto \min \left\{ (\mathbf{t} - \mathbf{A}\mathbf{s}_g)^T \mathbf{\Sigma}_\epsilon^{-1} (\mathbf{t} - \mathbf{A}\mathbf{s}_g) + (\mathbf{s}_g - \mathbf{s}_s)^T \mathbf{\Sigma}_g^{-1} (\mathbf{s}_g - \mathbf{s}_s) \right. \\ &\quad \left. + \sum_i (\mathbf{D}\mathbf{x}_i - \mathbf{R}_i \mathbf{s}_s)^T \mathbf{\Sigma}_{p,i}^{-1} (\mathbf{D}\mathbf{x}_i - \mathbf{R}_i \mathbf{s}_s) \right\} \\ &\quad \text{subject to } \|\mathbf{x}_i\|_0 = T \forall i. \end{aligned} \quad (11)$$

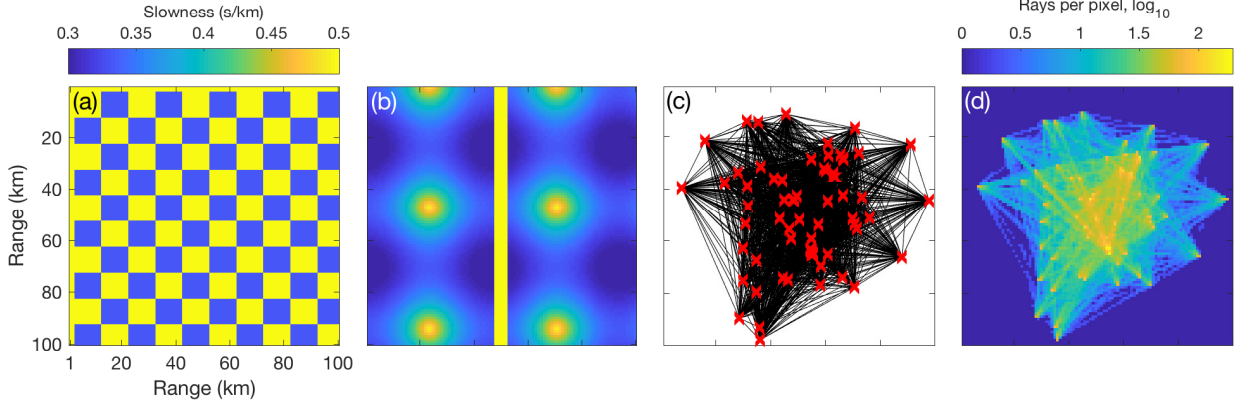


Fig. 3. Synthetic slowness maps and ray sampling. Slowness \mathbf{s}' for (a) checkerboard map and (b) smooth-discontinuous map (sinusoidal variations with discontinuity). Both maps are $W_1 = W_2 = 100$ pixels (1 km/pixel). (c) 64 stations (red X's), giving in 2016 straight ray (surface wave) paths through synthetic images. (d) Density of ray sampling, in \log_{10} rays per pixel.

Further simplifying, we assume the errors are Gaussian iid. Thus, $\Sigma_\epsilon = \sigma_\epsilon^2 \mathbf{I}$, $\Sigma_g = \sigma_g^2 \mathbf{I}$, and $\Sigma_{p,i} = \sigma_{p,i}^2 \mathbf{I}$, where \mathbf{I} is the identity matrix. The MAP estimate $\{\hat{\mathbf{s}}_g, \hat{\mathbf{s}}_s, \hat{\mathbf{X}}\}$ is thus

$$\begin{aligned} \{\hat{\mathbf{s}}_g, \hat{\mathbf{s}}_s, \hat{\mathbf{X}}\} = \arg \min_{\mathbf{s}_g, \mathbf{s}_s, \mathbf{X}} & \left\{ \frac{1}{\sigma_\epsilon^2} \|\mathbf{t} - \mathbf{A}\mathbf{s}_g\|_2^2 \right. \\ & \left. + \frac{1}{\sigma_g^2} \|\mathbf{s}_g - \mathbf{s}_s\|_2^2 + \frac{1}{\sigma_{p,i}^2} \sum_i \|\mathbf{D}\mathbf{x}_i - \mathbf{R}_i \mathbf{s}_s\|_2^2 \right\} \quad (12) \\ & \text{subject to } \|\mathbf{x}_i\|_0 = T \forall i. \end{aligned}$$

A. Solving for the MAP estimate

We find the MAP estimates $\{\hat{\mathbf{s}}_g, \hat{\mathbf{s}}_s, \hat{\mathbf{X}}\}$ solving (12) via a block-coordinate minimization algorithm [7], [20]. The objective for \mathbf{s} is written from (12) as

$$\begin{aligned} \hat{\mathbf{s}}_g &= \arg \min_{\mathbf{s}_g} \frac{1}{\sigma_\epsilon^2} \|\mathbf{t} - \mathbf{A}\mathbf{s}_g\|_2^2 + \frac{1}{\sigma_g^2} \|\mathbf{s}_g - \mathbf{s}_s\|_2^2 \\ &= \arg \min_{\mathbf{s}_g} \|\mathbf{t} - \mathbf{A}\mathbf{s}_g\|_2^2 + \lambda_1 \|\mathbf{s}_g - \mathbf{s}_s\|_2^2, \end{aligned} \quad (13)$$

where $\lambda_1 = (\sigma_\epsilon/\sigma_g)^2$ is a regularization parameter.

The local objective from (12) for each patch is solved with $\mathbf{s}_s = \hat{\mathbf{s}}_g$ (decoupling the local and global problems), giving

$$\hat{\mathbf{x}}_i = \arg \min_{\mathbf{x}_i} \|\mathbf{D}\mathbf{x}_i - \mathbf{R}_i \hat{\mathbf{s}}_g\|_2^2 \quad \text{subject to } \|\mathbf{x}_i\|_0 = T. \quad (14)$$

With the estimate of coefficients $\hat{\mathbf{X}} = [\hat{\mathbf{x}}_1, \dots, \hat{\mathbf{x}}_I]$ from (14) and global slowness $\hat{\mathbf{s}}_g$ from (13) we solve for \mathbf{s}_s . (12) gives, assuming constant patch variance $\sigma_{p,i}^2 = \sigma_p^2$,

$$\begin{aligned} \hat{\mathbf{s}}_s &= \arg \min_{\mathbf{s}_s} \frac{1}{\sigma_g^2} \|\hat{\mathbf{s}}_g - \mathbf{s}_s\|_2^2 + \frac{1}{\sigma_p^2} \sum_i \|\mathbf{D}\hat{\mathbf{x}}_i - \mathbf{R}_i \mathbf{s}_s\|_2^2 \\ &= \arg \min_{\mathbf{s}_s} \lambda_2 \|\hat{\mathbf{s}}_g - \mathbf{s}_s\|_2^2 + \sum_i \|\mathbf{D}\hat{\mathbf{x}}_i - \mathbf{R}_i \mathbf{s}_s\|_2^2, \end{aligned} \quad (15)$$

where $\lambda_2 = (\sigma_p/\sigma_g)^2$ is a regularization parameter. The estimate $\hat{\mathbf{s}}_s$ is obtained analytically by differentiating (15)

$$\begin{aligned} \frac{d}{d\mathbf{s}_s} & \left\{ \lambda_2 \|\hat{\mathbf{s}}_g - \mathbf{s}_s\|_2^2 + \sum_i \|\mathbf{D}\hat{\mathbf{x}}_i - \mathbf{R}_i \mathbf{s}_s\|_2^2 \right\} \\ &= \lambda_2 (\mathbf{s}_s - \hat{\mathbf{s}}_g) + \sum_i \mathbf{R}_i^T (\mathbf{R}_i \mathbf{s}_s - \mathbf{D}\hat{\mathbf{x}}_i) \\ &= (\lambda_2 \mathbf{I} + \sum_i \mathbf{R}_i^T \mathbf{R}_i) \mathbf{s}_s - \lambda_2 \hat{\mathbf{s}}_g - \sum_i \mathbf{R}_i^T \mathbf{D}\hat{\mathbf{x}}_i = \mathbf{0}. \end{aligned} \quad (16)$$

Thus, \mathbf{s}_s is

$$\hat{\mathbf{s}}_s = \left(\lambda_2 \mathbf{I} + \sum_i \mathbf{R}_i^T \mathbf{R}_i \right)^{-1} \left(\lambda_2 \hat{\mathbf{s}}_g + \sum_i \mathbf{R}_i^T \mathbf{D}\hat{\mathbf{x}}_i \right). \quad (17)$$

which averages the pixels from the patch estimates $\{\mathbf{D}\hat{\mathbf{x}}_i \forall i\}$, with weight given to $\hat{\mathbf{s}}_g$ by λ_2 . From (17), the average patch slowness is $\mathbf{s}_p = \left(\sum_i \mathbf{R}_i^T \mathbf{R}_i \right)^{-1} \left(\sum_i \mathbf{R}_i^T \mathbf{D}\hat{\mathbf{x}}_i \right)$, with $\mathbf{b} = \text{diag}(\sum_i \mathbf{R}_i^T \mathbf{R}_i) \in \mathbb{Z}^N$ the number of patches per pixel. Hence, (17) is expressed as an operation at pixel n by

$$\hat{\mathbf{s}}_{s,n} = \frac{\lambda_2 \hat{\mathbf{s}}_{g,n} + \mathbf{b}_n \mathbf{s}_{p,n}}{\lambda_2 + \mathbf{b}_n}. \quad (18)$$

The values of \mathbf{b}_n are $1 \leq \mathbf{b}_n \leq n$, with $\mathbf{b}_n = n$ is obtained at $\geq \sqrt{n}$ pixels from the edge of slowness map (see Fig. 1(b)).

B. LST algorithm with dictionary learning

The expressions (13), (14), and (18) are solved iteratively, giving the LST algorithm as a MAP estimate of a slowness image with local sparse constraints with a known dictionary \mathbf{D} . Dictionary learning is added to the algorithm in the solution to the local problem (14). Dictionary learning in this paper is accomplished using the ITKM algorithm, Table II).

For fixed sparsity T , the ITKM [6] is more computationally efficient and has better guarantees of dictionary recovery than the classic K-SVD algorithm [5]. It solves (14) using thresholding, and phrases the optimization of \mathbf{D} using a 'signed' K-means objective. The ITKM is summarized in Table II, with details in Appendix A.

Since \mathbf{A} is sparse, the global estimate (13) is solved using the sparse least squares program LSQR [35]. The local

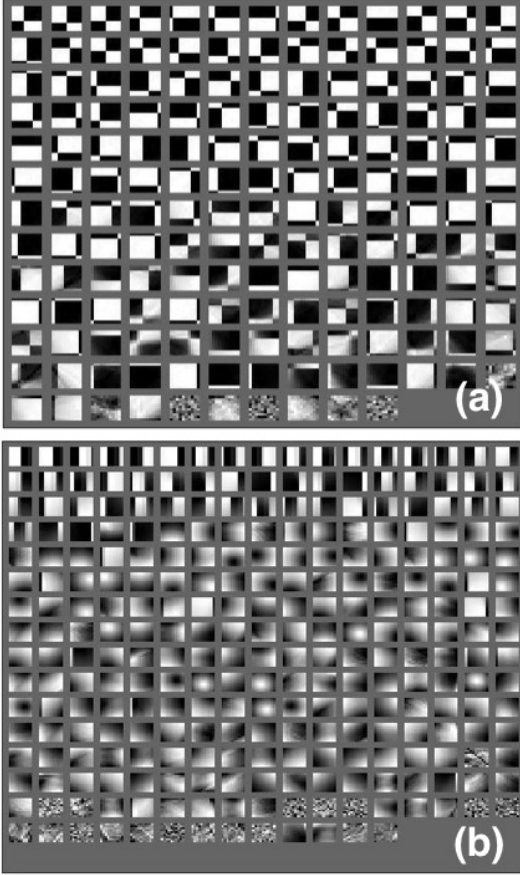


Fig. 4. Dictionary atoms learned during LST with ITKM, with $n = 100$ and $T = 1$ nonzero coefficient for (a) checkerboard map (Fig. 3(a)) with $Q = 166$ and (b) smooth-discontinuous map (Fig. 3(b)) with $Q = 268$. Atoms stretched to full grayscale range for display.

estimate (14) is solved using orthogonal matching pursuit (OMP) [36] after the slowness patches $\{\mathbf{R}_i \widehat{\mathbf{s}}_g \forall i\}$ are centered [4] – i.e. the mean of the pixels in each patch is subtracted. The mean of patch i is $\bar{x}_i = \frac{1}{n} \mathbf{1}^T \mathbf{R}_i \widehat{\mathbf{s}}_g$. Hence, $\mathbf{R}_i \widehat{\mathbf{s}}_g \approx \mathbf{D} \mathbf{x}_i + \mathbf{1} \bar{x}_i$. The algorithm for the MAP estimate with and without dictionary learning is given in Table I.

To illustrate the content of learned dictionaries, the dictionary atoms learned during the inversion of the checkerboard are shown in Fig. 4(a) and for the smooth-discontinuous map in Fig. 4(b).

C. Conventional tomography

We illustrate conventional tomography with a Bayesian approach [37], which enforces smoothness regularization with a global (non-diagonal) covariance. Considering the measurements (1), the MAP estimate of the slowness is

$$\widehat{\mathbf{s}}_g = (\mathbf{A}^T \mathbf{A} + \eta \Sigma_L^{-1})^{-1} \mathbf{A}^T \mathbf{t}, \quad (19)$$

where $\eta = (\sigma_\epsilon / \sigma_c)^2$ is a regularization parameter, σ_c is the conventional slowness variance, and

$$\Sigma_L(i, j) = \exp(-D_{i,j}/L). \quad (20)$$

Here $D_{i,j}$ is the distance between cells i and j , and L is the smoothness length scale [10], [37].

TABLE I
LOCALLY-SPARSE TRAVEL TIME TOMOGRAPHY (LST) ALGORITHM

Given: $\mathbf{t} \in \mathbb{R}^K$, $\mathbf{A} \in \mathbb{R}^{M \times N}$, $\mathbf{s}_s^0 = \mathbf{0} \in \mathbb{R}^N$, $\mathbf{D}^0 =$ Haar wavelet, DCT (or) noise $\mathcal{N}(0, 1) \in \mathbb{R}^{n \times Q}$, λ_1, λ_2, T , and $j = 1$
Repeat until convergence:
1. Global estimate: solve (13) using LSQR [35], $\widehat{\mathbf{s}}_g^j = \arg \min_{\mathbf{s}_g^j} \ \mathbf{A} \mathbf{s}_g^j - \mathbf{t}\ _2^2 + \lambda_1 \ \mathbf{s}_g^j - \mathbf{s}_g^{j-1}\ _2^2.$
2. Local estimate
a: Setting $\mathbf{s}_i^j = \widehat{\mathbf{s}}_g^j$, center patches $\{\mathbf{R}_i \widehat{\mathbf{s}}_g^j \forall i\}$ and
i. (Dictionary learning) Find \mathbf{D}^j using ITKM [6] (Table II).
ii. (generic dictionary) Set $\mathbf{D}^j = \mathbf{D}^0$.
iii. Solve (14) using OMP, $\widehat{\mathbf{x}}_i^j = \arg \min_{\mathbf{x}_i^j} \ \mathbf{D}^j \mathbf{x}_i^j - \mathbf{R}_i \widehat{\mathbf{s}}_g^j\ _2^2 \text{ subject to } \ \mathbf{x}_i^j\ _0 = T.$
b: Obtain $\widehat{\mathbf{s}}_g^j$ by (18) $\forall w$, $\widehat{s}_{s,w}^j = \frac{\lambda_2 \widehat{s}_{g,w}^j + s_{p,w}^j}{\lambda_2 + b_w}$
$j = j + 1$

TABLE II
ITKM ALGORITHM

Given: $j, \widehat{\mathbf{s}}_g^j, \mathbf{D}^0 = \mathbf{D}^{j-1} \in \mathbb{R}^{n \times Q}$, T , and $h = 1$
Repeat until convergence:
1. Find dictionary indices per (25) $K(\mathbf{D}^{h-1}, \mathbf{y}_i) = \max_{ K =T} \ \mathbf{D}_K^{h-1 T} \mathbf{y}_i\ _1,$ with $\mathbf{y}_i = \mathbf{R}_i \widehat{\mathbf{s}}_g^j - \mathbf{1} \bar{x}_i^j$.
2. Update dictionary per (30) using coefficient indices K $\mathbf{d}^h = \lambda_l \sum_{i:l \in K(\mathbf{D}^{h-1}, \mathbf{y}_i)} \text{sign}(\mathbf{d}_l^{h-1 T} \mathbf{y}_i) \mathbf{y}_i$ with λ_l such that $\ \mathbf{d}_l^h\ _2 = 1$. $h = h + 1$
Output: $\mathbf{D}^j = \mathbf{D}^h$

IV. SIMULATIONS

We demonstrate the performance of LST (Sec. III, Table I) relative to conventional tomography (Sec. III-C), with results summarized in Table III. Experiments are conducted using simulated seismic data from two synthetic 2D seismic slowness maps (Fig. 3(a–b)) with dimensions $W_1 = W_2 = 100$ pixels (km). The boxcar checkerboard in Fig. 3(a) demonstrates the recovery of discontinuous seismic slownesses. The smooth-discontinuous map Fig. 3(b) illustrates fault-like discontinuities in an otherwise smoothly varying (sinusoidal) slowness map, as used in [15]. This example illustrates the modeling flexibility of the LST algorithm. The slowness estimates from LST are $\widehat{\mathbf{s}}_s^j = \widehat{\mathbf{s}}_s + \mathbf{s}_0 \in \mathbb{R}^N$ (from (18)), and for conventional $\widehat{\mathbf{s}}_s^j = \widehat{\mathbf{s}}_s + \mathbf{s}_0 \in \mathbb{R}^N$ (from (19)).

For the slowness map pixels are 1 km square and sampled by $M = 2016$ straight-rays between 64 seismic stations, shown in Fig. 3(c). The travel times \mathbf{t} is calculated by numerically integrating along these ray paths. The 2D valid-region for the slowness map estimates is determined for the LST by a dilation operation with a patch template along the outermost ray paths in Fig. 3(c). The conventional tomography valid region is bounded by the outermost pixels along the ray paths. The conventional tomography valid region is used for error calculations for both conventional and LST.

To avoid overfitting during dictionary learning (Table II), we exclude patches if more than 10 % of the pixels are

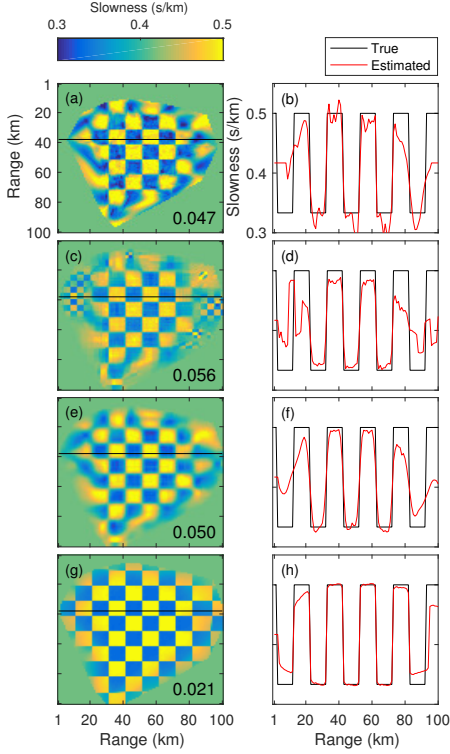


Fig. 5. LST and conventional tomography without travel time error for checkerboard map (Fig. 3(a)). 2D and 1D (from black line in 2D) slowness estimates against true slowness s' for: (a,b) conventional \widehat{s}'_g from with $L = 10$ km and $\eta = 0.1$ km²; LST \widehat{s}'_s for $\lambda_1 = 0$ km², $\lambda_2=0$, $n = 100$ with (c,d) Haar wavelet and (e,f) DCT dictionary with $Q = 169$, $T = 2$ and $n = 64$; and (g,h) with dictionary learning for $Q = 166$ and $T = 1$.

not sampled by ray paths. This heuristic works well and we have not investigated dictionary learning from incomplete information. The RMSE (s/km) of the estimates is calculated by

$$\text{RMSE} = \sqrt{\frac{1}{NP} \sum_n^N \sum_p^P (s'_{np} - s'_{\text{est},np})^2}, \quad (21)$$

where $s'_{\text{est},np}$ is \widehat{s}'_s or \widehat{s}'_g for the n -th pixel location, and the p -th trial. For $\sigma_\epsilon = 0$, $P = 1$. The RMSE is printed on the 2D slowness images in Figs. 5–8, 11–12, and on the 1D profiles in Figs. 9 and 10.

A. Without travel time error

We first simulate travel times without errors ($\sigma_\epsilon = 0$) to obtain best-case results for the LST and conventional tomography. See Figs. 5 and 6 for results for LST and conventional tomography. For the LST we invert the travel time using the algorithm in Table I both with and without dictionary learning. For the case with no dictionary learning, the dictionary \mathbf{D} is either the overcomplete Haar wavelet dictionary or the DCT (see Fig. 2). RMSE performance is in Table III.

1) *Inversion parameters for $\sigma_\epsilon = 0$* : The LST tuning parameters are λ_1 , λ_2 , n , Q , and T . The sensitivity of the LST solutions with dictionary learning to λ_1 and λ_2 are shown in Fig. 8 for nominal values of $n = 100$, $Q = 166$ ($Q = 268$) for

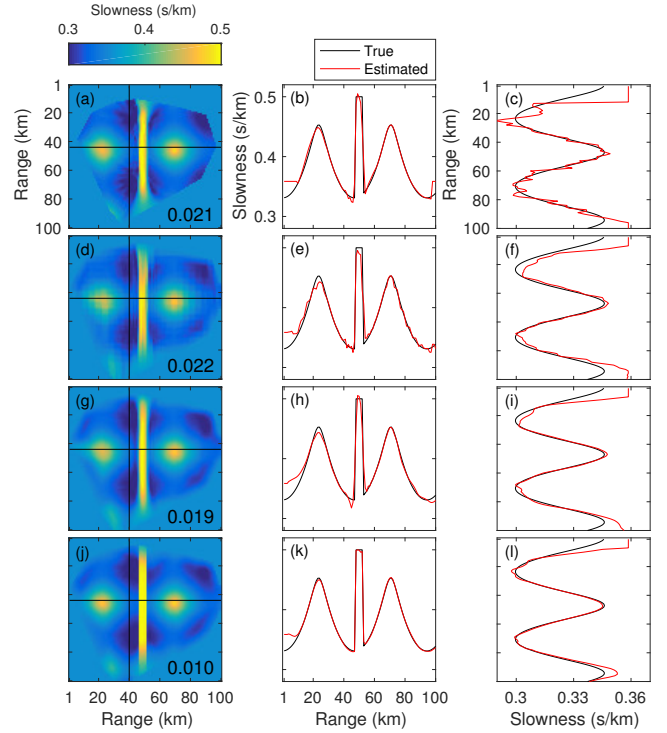


Fig. 6. LST and conventional tomography without travel time error for smooth-discontinuous map (Fig. 3(b)). 2D and 1D (from black lines in 2D) slowness estimates against true slowness s' for: (a–c) conventional \widehat{s}'_g from with $L = 10$ km and $\eta = 0.1$ km²; LST \widehat{s}'_s for $\lambda_1 = 0$ km², $\lambda_2=0$, $n = 100$ with (c,d) Haar wavelet and (e,f) DCT dictionary with $Q = 169$, $T = 2$, and $n = 64$; and (g,h) with dictionary learning for $Q = 268$ and $T = 1$.

the checkerboard (smooth-discontinuous), and $T = 1$. With the prior $\sigma_\epsilon = 0$ s, we expect the best value of $\lambda_1 = 0$ km² (from (13)). From (13), (15) σ_g^2 is proportional to the variance of the true slowness, which for the checkerboard (smooth-discontinuous) is 0.013 (0.025) s²/km². We assume the slowness patches are well approximated by the sparse model (14), and expect $\sigma_p^2 \ll \sigma_g^2$. Hence we expect the best value of λ_2 (from (15)) to be small. It is shown for both the checkerboard (Fig. 8(a)) and smooth-discontinuous maps (Fig. 8(b)) that the best RMSE for the LST with dictionary learning is obtained when $\lambda_1 = 0$ km² and $\lambda_2 = 0$, though the LST exhibits low sensitivity to these values and recovers well the true slowness for a large range of values.

For the LST with the Haar wavelet and DCT dictionaries (both $Q = 169$, $n = 64$, since Haar wavelet dimensions power of 2), the best performance by minimum RMSE was achieved for both the checkerboard and smooth-discontinuous maps with $\lambda_1 = 0$ km², $\lambda_2 = 0$, and $T = 2$.

Several methods exist for estimating the best regularization parameters L and η in conventional tomography [2], but are not always reliable [38]. To find the best parameters, we systematically varied the values of L and η (see Fig. 7). The best RMSE for conventional tomography was obtained by $L = 10$ km and $\eta = 0.1$ km² for both the checkerboard and smooth-discontinuous maps.

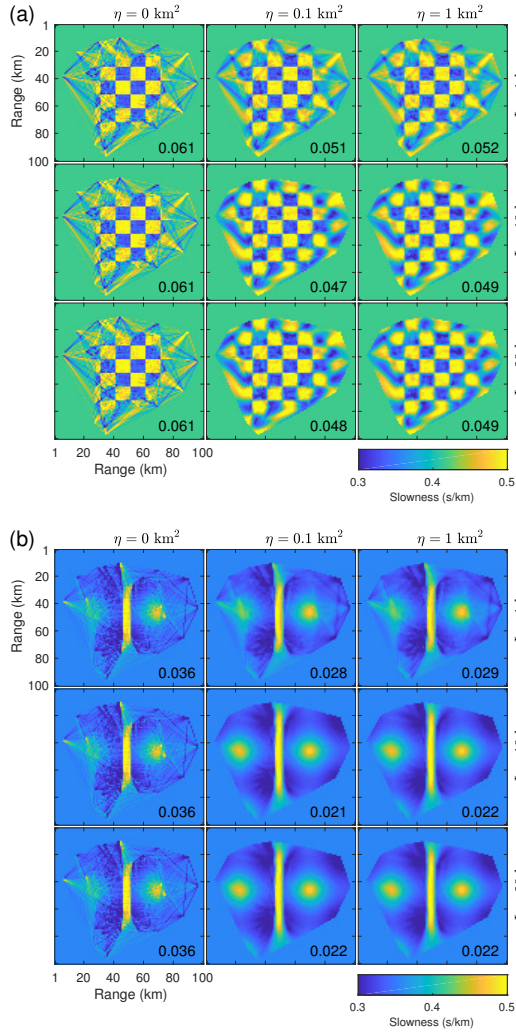


Fig. 7. Conventional tomography $\hat{\mathbf{s}}_g'$ without travel time error for different values of regularization parameters η and L for (a) checkerboard (Fig. 3(a)) and (b) smooth-discontinuous (Fig. 3(b)) maps.

2) *Results for $\sigma_\epsilon = 0$* : While the discontinuous shapes in the Haar dictionary are similar to the discontinuous content of the checkerboard image, the local features in the higher order Haar wavelets overfit the rays where the ray sampling density is poor (see Fig. 3(d)). The performance of the Haar wavelets is better for the smooth-discontinuous slowness map (Fig. 6(d–f)) than for the checkerboard. As shown in Fig. 6(d–f), the Haar wavelets add false high frequency structure to the slowness reconstruction but the trends in the smooth-discontinuous features are well preserved. The inversion performance of the DCT transform (Fig. 5(e,f) and Fig. 6(g,j)) is better than the Haar wavelets for both cases, but matches less closely the discontinuous slowness features, as the DCT atoms are smooth. The smoothness of the DCT atoms better preserve the smooth slowness structure.

The LST with dictionary learning (Fig. 5(g,h) and Fig. 6(j–l)) achieves the best overall fit to the true slowness, recovering nearly exactly the true slownesses. As in the other cases, the performance degrades near the edges of the ray sampling, where the ray density is low, but high resolution is

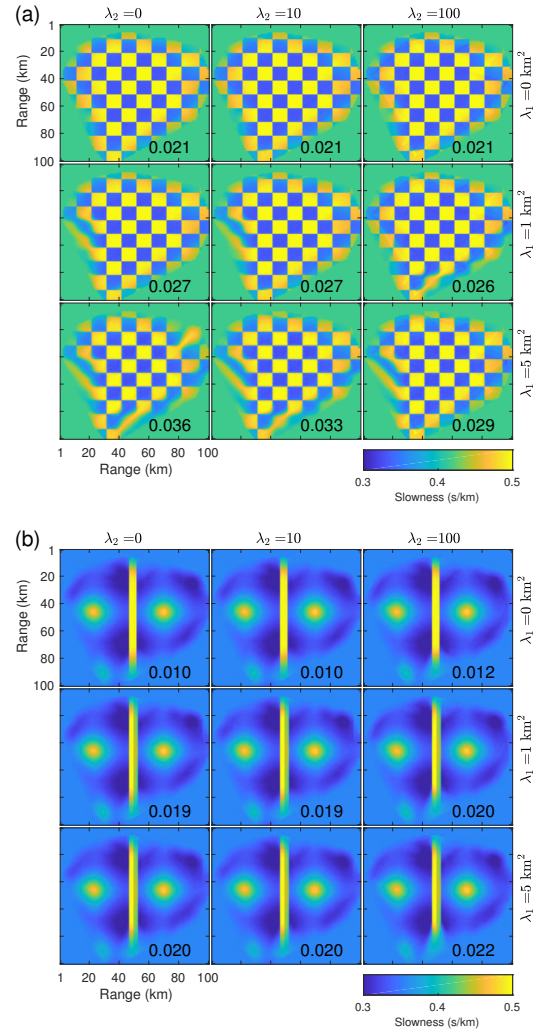


Fig. 8. LST $\hat{\mathbf{s}}_g'$ without travel time error for different values of regularization parameters λ_1 and λ_2 for $n = 100$ and $T = 1$ (a) checkerboard $Q = 166$ (Fig. 3(a)) and (b) smooth-discontinuous $Q = 268$ (Fig. 3(b)) maps.

maintained across a large part of the sampling region. The RMSE of the LST with both the Haar wavelet and DCT dictionaries for the checkerboard (Table III) is greater than for conventional tomography, although a better qualitative fit to the true slowness is observed with the LST.

The true variances σ_ϵ , σ_g , and σ_p in the LST regularization parameters λ_1 and λ_2 provide best LST performance (see Fig. 8), whereas the true variances for conventional tomography, σ_ϵ and σ_c , do not correspond to the best solutions (see Fig. 7). The noise-free prior, $\eta = 0 \text{ km}^2$, gives erratic inversions, and the conventional tomography is better regularized by $\eta = 0.1 \text{ km}^2$.

B. With travel time error

We also simulate the inversions with travel time errors. We consider the case when $\sigma_\epsilon = 0.02\bar{t}$, or the uncertainty is 2% of the mean travel time, which is similar to the model implemented in [14]. For each true slowness map and method, we run the inversions for 100 realizations of noise $\mathcal{N}(0, \sigma_\epsilon)$ (also

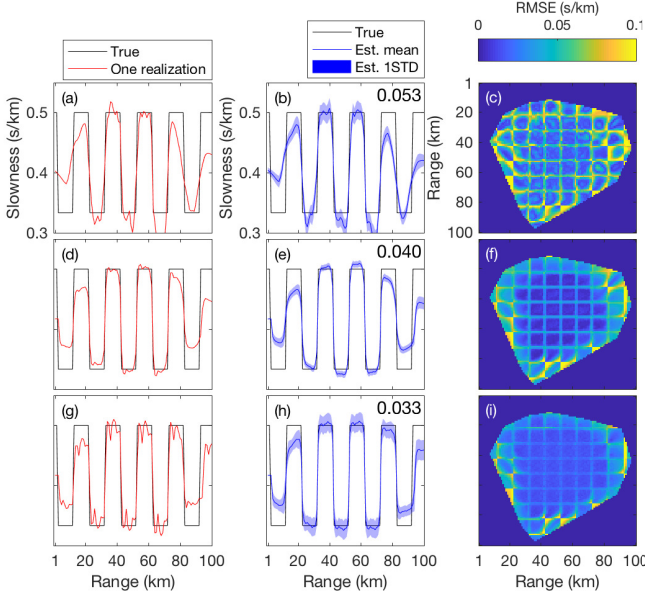


Fig. 9. LST and conventional tomography of checkerboard map (Fig. 3(a)) for 100 realizations of Gaussian travel time error with STD of 2% mean travel time. 1D slice of inversion (same location as Fig. 5) for one noise realization against true slowness, 1D slice of mean from over all noise realizations with STD of estimate against true slowness s' , and 2D RMSE of estimates over noise realizations for: (a–c) conventional tomography \hat{s}'_g with $L = 6$ km and $\eta = 10$ km²; LST \hat{s}'_g with dictionary learning for (d–f) $\lambda_1 = 10$ km² and (g–i) $\lambda_1 = 5$ km², with $\lambda_2 = 0$, $n = 100$, $Q = 144$, and $T = 1$.

TABLE III
LST AND CONVENTIONAL TOMOGRAPHY RMSE PERFORMANCE

Error $\sigma_\epsilon =$	RMSE (s/km)			
	Checkerboard		Smooth-discon.	
	0*	0.02 \bar{t} **	0 \dagger	0.02 \bar{t} $\dagger\dagger$
LST Haar	0.056	–	0.022	–
LST DCT	0.050	–	0.019	–
LST Adaptive	0.021	0.033	0.010	0.020
Conventional	0.047	0.053	0.021	0.026

*Fig. 5, **Fig. 9, \dagger Fig. 6, and $\dagger\dagger$ Fig 10.

the random initialization of \mathbf{D} also changes 100 times) and summarize the statistics of the results. The noise simulation results for the LST and conventional tomography are in Figs. 9 and 10. For the LST, we invert the travel time using the algorithm in Table I only with dictionary learning. The RMSE for both approaches, calculated by (21) with $P = 100$, are in Table III.

1) *Inversion parameters for $\sigma_\epsilon = 0.02\bar{t}$* : The sensitivity of the LST solutions with dictionary learning to λ_1 and λ_2 are shown in Fig. 12 for nominal values of $n = 100$, $Q = 144$ ($Q = 100$), and $T = 1$ ($T = 2$) for the checkerboard (smooth-discontinuous). With the prior $\sigma_\epsilon = 0.02\bar{t}$, we expect for the checkerboard map ($\sigma_\epsilon = 0.28$ s, $\sigma_g = 0.11$ s/km) the best value of $\lambda_1 \approx 6.5$ km², and for the the smooth-discontinuous ($\sigma_\epsilon = 0.25$ s, $\sigma_g = 0.16$ s/km) the best value of $\lambda_1 \approx 2.4$ km² (from (13)). We use $\lambda_1 = 5$ km² for both cases in Figs. 9 and 10, and achieve lower RMSE than $\lambda_1 = 1$ km² or $\lambda_1 = 10$ (see Fig. 12). Although we expect the true values σ_g to decrease over the LST iterations, prior values of σ_g proportional to the variance of the true slowness work well. It is further shown

in Fig. 12 that, as in the the noise-free case (Sec. IV-A1), the LST recovers well the true slowness for a large range of values.

For conventional tomography, the best values by minimum RMSE were $L = 6$ km and $\eta = 10$ km² for both the checkerboard and the smooth-discontinuous slowness maps.

Considering again the influence of the choice of λ_1 and λ_2 on the LST in Fig. 12, since $b_n = 100$ for these examples, the case $\lambda_2 = 100$ gives equal weight to the global $\hat{s}_{g,n}$ and patch slowness $b_n s_{p,n}$ in (18). The LST obtains similar RMSE to the best conventional estimates (see Fig. 11) for the checkerboard with $\lambda_1 = 1$ and $\lambda_2 = 100$ and for the smooth-discontinuous map with $\lambda_1 = 10$ and $\lambda_2 = 500$, though these parameters are suboptimal. Though in this case, the sparsity regularization of the patches has an effect similar to the conventional damping and smoothing regularization from (19), there is no direction relationship between the regularization in (19) and the sparsity and dictionary learning in (14).

2) *Results for $\sigma_\epsilon = 0.02\bar{t}$* : The LST with dictionary learning (Fig. 9(g–i) and Fig. 10(e–h)) achieves the best overall fit to the true slowness, relative to conventional tomography (Fig. 9(a–c) and Fig. 10(a–d)) as evidenced by qualitative fit and RMSE (Table III). In the case of the checkerboard, a higher value $\lambda_1 = 10$ is tested and shown in Fig. 9(d–f). Because of the increased damping, the standard deviation (STD) of the estimate (Fig. 9(e)) is less than the case $\lambda_1 = 5$ km² (Fig. 9(b)), and fit to true profile is improved.

As in the noise-free case, LST regularization parameters λ_1 and λ_2 proportional to the true variances provide best LST performance (see Fig. 12), whereas true variances for conventional tomography do not correspond to the best solutions (see Fig. 7).

3) *Convergence and run time*: The algorithms were coded in Matlab. The LST algorithm (Table I) used 100 iterations for all cases and the ITKM (Table II) used 50 iterations. As an example of run time, the inversion with dictionary learning in Fig. 5(g,h) took 5 min on a Macbook Pro 2.5 GHz Intel Core i7 and with dictionary learning in Fig. 6(j–l) took 6 min. The RMSE travel time error for the slowness model s_s decreased over the iterations and converged within at most 50 iterations (see Fig. 13). For the cases with travel time uncertainty, the RMSE approaches or falls only slightly below σ_ϵ . Hence, the travel time data was not overfit.

V. CONCLUSIONS

We have derived a method for travel time tomography which incorporates a local sparse prior on patches of the slowness image, which we refer to as the LST algorithm. The LST can use predefined or learned dictionaries, though learned dictionaries gives improved performance. Relative to the conventional tomography method presented, the LST is less sensitive the regularization parameters. LST with sparse prior and dictionary learning can solve for both smooth and discontinuous slowness features in an image.

We considered the case of 2D surface wave tomography and, for the dense sampling configuration and synthetic images we used, obtained good recovery of true slowness maps with

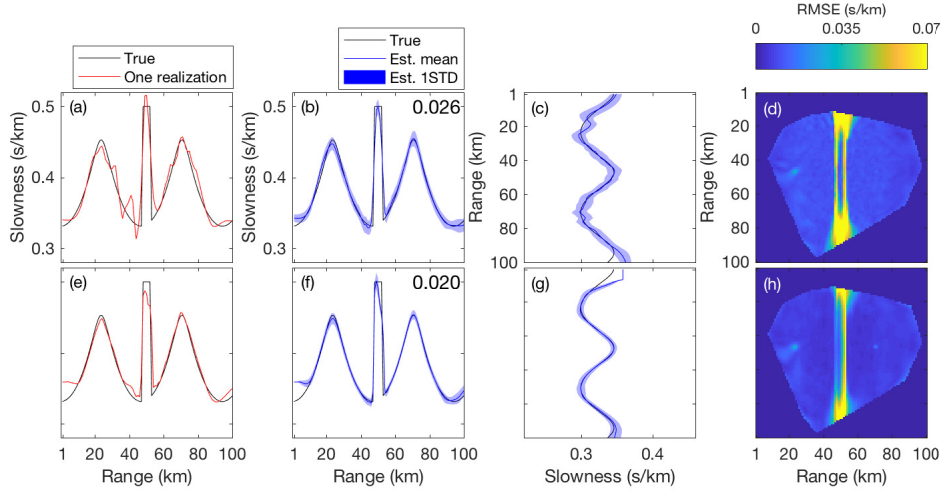


Fig. 10. LST and conventional tomography of smooth-discontinuous map (Fig. 3(b)) for 100 realizations of Gaussian travel time error with STD of 2% mean travel time. Horizontal 1D slice of inversion (same locations as Fig. 6) for one noise realization against true slowness, horizontal and vertical 1D slice of mean from over all noise realizations with STD of estimate against true slowness s' , and 2D RMSE of estimates over noise realizations for: (a–d) conventional tomography \hat{s}_g with $L = 12$ km and $\eta = 10$ km²; (e–h) LST \hat{s}_g with dictionary learning with $\lambda_1 = 5$ km², $\lambda_2 = 0$, $n = 100$, $Q = 100$, and $T = 2$.

exclusively discontinuous features as well as smooth and discontinuous features. The LST is relevant to other tomography scenarios where slowness structure is irregularly sampled, in for instance ocean [39] and terrestrial [40], [41] acoustics.

APPENDIX

A. ITKM algorithm details

The ITKM dictionary learning algorithm [6] (see Table II) is derived from a ‘signed’ K-means objective. In signed K-means, T -sparse coefficients $\mathbf{C} = [\mathbf{c}_1, \dots, \mathbf{c}_T] \in \mathbb{R}^{Q \times I}$ with $\mathbf{c}_i^T \in \{-1, 1\}$ are assigned to training examples $\{\mathbf{y}_1, \dots, \mathbf{y}_I\} \in \mathbb{R}^{n \times I}$. The training examples in this paper obtained from patch i as $\mathbf{y}_i = \mathbf{R}_i \mathbf{u}$, and centered. The minimization problem is

$$\begin{aligned} \{\mathbf{C}, \mathbf{D}\} &= \arg \min_{\mathbf{D}} \sum_i \arg \min_{T, \mathbf{c}_i^T = \pm 1} \|\mathbf{y}_i - \mathbf{D} \mathbf{c}_i\|_2^2 \\ &= \min_{\mathbf{D}} \sum_i \min_{T, \mathbf{c}_i^T = \pm 1} \|\mathbf{y}_i - \sum_t \mathbf{d}_t c_i^t\|_2^2, \end{aligned} \quad (22)$$

where c_i^t is a non-zero coefficient and \mathbf{d}_t is the corresponding dictionary entry. Expanding (22),

$$\begin{aligned} \{\mathbf{C}, \mathbf{D}\} &= \min_{\mathbf{D}} \sum_i \min_{T, \mathbf{c}_i^T = \pm 1} \left\{ \mathbf{y}_i^T \mathbf{y}_i - 2 \sum_t c_i^t \mathbf{d}_t^T \mathbf{y}_i \right. \\ &\quad \left. + (c_i^t)^2 \left(\sum_t \mathbf{d}_t^T \mathbf{d}_t + 2 \sum_{u < t} \mathbf{d}_u^T \mathbf{d}_t \right) \right\}. \end{aligned} \quad (23)$$

Simplifying (23), requiring $\|\mathbf{d}_t\|_2^2 = 1$,

$$\begin{aligned} &\min_{\mathbf{D}} \sum_i \min_{T, \mathbf{c}_i^T = \pm 1} \left\{ \|\mathbf{y}_i\|_2^2 - 2 \sum_t c_i^t \mathbf{d}_t^T \mathbf{y}_i + B \right\} \\ &= \|\mathbf{Y}\|_{\mathcal{F}}^2 + B - 2 \max_{\mathbf{D}} \sum_i \max_{|K|=T} \sum_t \|\mathbf{d}_t^T \mathbf{y}_i\|_1 \\ &= \|\mathbf{Y}\|_{\mathcal{F}}^2 + B - 2 \max_{\mathbf{D}} \sum_i \max_{|K|=T} \|\mathbf{D}_K^T \mathbf{y}_i\|_1, \end{aligned} \quad (24)$$

where B is a constant, and K is the set of T dictionary indices having the largest absolute inner product $\|\mathbf{d}_t \mathbf{y}_i\|_1$, by

$$K(\mathbf{D}, \mathbf{y}_i) = \max_{|K|=T} \|\mathbf{D}_K^T \mathbf{y}_i\|_1. \quad (25)$$

In contrast to OMP [36], (25) is the thresholding [3] solution to (14). From (24) it is seen that the dictionary learning objective is

$$\max_{\mathbf{D}} \sum_i \max_{|K|=T} \|\mathbf{D}_K^T \mathbf{y}_i\|_1, \quad (26)$$

which finds \mathbf{D} that maximizes the absolute norm of the T -largest responses from K .

The ITKM obtains dictionary learning by solving (26) as a two-step algorithm. First, K is obtained from (25). Then, the dictionary atoms are updated per

$$\max_{\mathbf{D}} \sum_{i: l \in K(\mathbf{D}, \mathbf{y}_i)} \|\mathbf{d}_l^T \mathbf{y}_i\|_1, \quad (27)$$

which is solved using Lagrange multipliers, with the constraint $\|\mathbf{d}_l\|_2 = 1$. From (27),

$$\frac{\partial}{\partial \mathbf{d}_l} \left(\sum_{i: l \in K(\mathbf{D}, \mathbf{y}_i)} \|\mathbf{d}_l^T \mathbf{y}_i\|_1 \right) = \sum_{i: l \in K(\mathbf{D}, \mathbf{y}_i)} \text{sign}(\mathbf{d}_l^T \mathbf{y}_i) \mathbf{y}_i \quad (28)$$

and from the norm constraint

$$\frac{\partial}{\partial \mathbf{d}_l} (\|\mathbf{d}_l\|_2^2) = 2 \mathbf{d}_l. \quad (29)$$

Relating (28) and (29), the dictionary atom \mathbf{d}_l is updated by

$$\mathbf{d}_l^{\text{new}} = \lambda_l \sum_{i: l \in K(\mathbf{D}^{\text{old}}, \mathbf{y}_i)} \text{sign}(\mathbf{d}_l^{\text{old}T} \mathbf{y}_i) \mathbf{y}_i, \quad (30)$$

where λ_l scales the update to enforce $\|\mathbf{d}_l\|_2 = 1$. The complexity of each ITKM iteration is dominated by matrix multiplication, of order $O(nQI)$, which is much less than K-SVD [5] which for each iteration calculates the singular value decomposition of a $n \times I$ matrix Q times. The implemented ITKM algorithm is given in Table II.

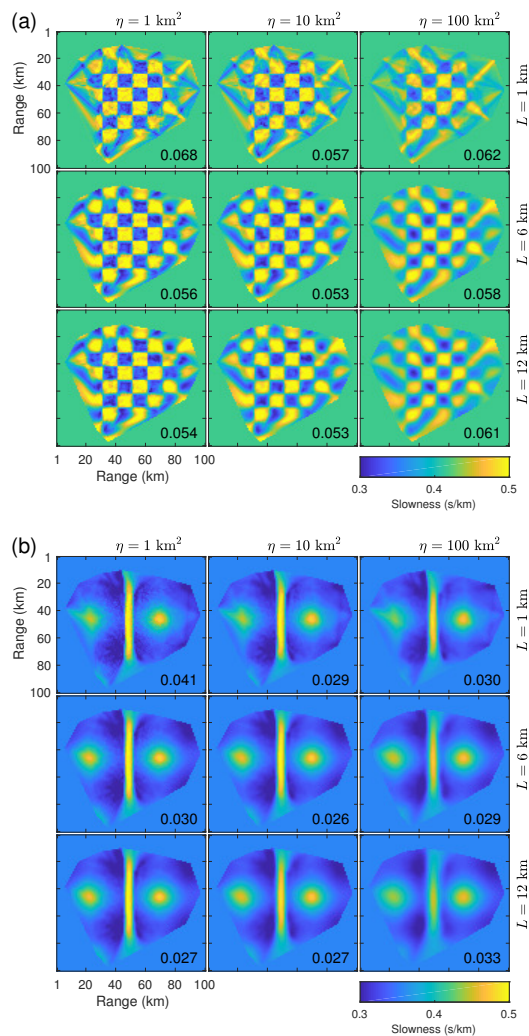


Fig. 11. Conventional tomography mean \hat{S}_g for 100 realizations of Gaussian travel time error with STD of 2% mean travel time for different values of regularization parameters η and L for (a) checkerboard (Fig. 3(a)) and (b) smooth-discontinuous (Fig. 3(b)) maps.

REFERENCES

- [1] N. Rawlinson, S. Pozgay, and S. Fishwick, "Seismic tomography: a window into deep earth," *Phys. Earth Plan. Inter.*, vol. 178, no. 3, pp. 101–135, 2010.
- [2] R. Aster, B. Borchers, and C. Thurber, *Parameter estimation and inverse problems*, 2nd ed. Elsevier, San Diego, 2013.
- [3] M. Elad, *Sparse and Redundant Representations*. Springer, New York, 2010.
- [4] J. Mairal, F. Bach, and J. Ponce, "Sparse modeling for image and vision processing," *Found. Trends Comput. Graph. Vis.*, vol. 8, no. 2–3, pp. 85–283, 2014.
- [5] M. Aharon, M. Elad, and A. Bruckstein, "K-SVD: An algorithm for designing overcomplete dictionaries for sparse representation," *IEEE Trans. Signal Process.*, vol. 54, pp. 4311–4322, 2006.
- [6] K. Schnass, "Local identification of overcomplete dictionaries," *J. Mach. Learn. Res.*, no. 16, pp. 1211–1242, 2015.
- [7] M. Elad and M. Aharon, "Image denoising via sparse and redundant representations over learned dictionaries," *IEEE Trans. Image Process.*, vol. 15, no. 12, pp. 3736–3745, 2006.
- [8] J. Mairal, F. Bach, J. Ponce, and G. Sapiro, "Online dictionary learning for sparse coding," *ACM Proc. 26th Inter. Conf. Mach. Learn.*, pp. 689–696, 2009.
- [9] J. Mairal, F. Bach, and J. Ponce, "Task-driven dictionary learning," *IEEE Trans. Pattern Anal. Mach. Intell.*, no. 4, pp. 791–804, 2012.
- [10] A. Tarantola, *Inverse problem theory*. Elsevier Sci. Pub. Co., Inc., 1987.
- [11] Y. Lin and L. Huang, "Quantifying subsurface geophysical properties changes using double-difference seismic-waveform inversion with a modified total-variation regularization scheme," *Geo. J. Int.*, vol. 203, no. 3, pp. 2125–2149, 2015.
- [12] X. Zhang and J. Zhang, "Model regularization for seismic traveltime tomography with an edge-preserving smoothing operator," *J. Appl. Geo.*, vol. 138, pp. 143–153, 2017.
- [13] L. Chiao and B. Kuo, "Multiscale seismic tomography," *Geo. J. Int.*, vol. 145, no. 2, pp. 517–527, 2001.
- [14] R. Hawkins and M. Sambridge, "Geophysical imaging using trans-dimensional trees," *Geo. J. Int.*, vol. 203, no. 2, pp. 972–1000, 2015.
- [15] I. Loris, G. Nolet, I. Daubechies, and F. Dahlen, "Tomographic inversion using ℓ_1 -norm regularization of wavelet coefficients," *Geo. J. Int.*, vol. 170, no. 1, pp. 359–370, 2007.
- [16] H. Fang and H. Zhang, "Wavelet-based double-difference seismic tomography with sparsity regularization," *Geo. J. Int.*, vol. 199, no. 2, pp. 944–955, 2014.
- [17] B. Olshausen and D. Field, "Sparse coding with an overcomplete basis set: a strategy employed by v1?" *Vis. Res.*, no. 37, pp. 3311–3325, 1997.
- [18] H. Taylor, S. Banks, and J. McCoy, "Deconvolution with the ℓ_1 -norm," *Geophys.*, vol. 44, no. 1, pp. 39–52, 1979.
- [19] M. Lustig, D. Donoho, and J. Pauly, "Sparse MRI: the application of compressed sensing for rapid MR imaging," *Mag. Res. Medic.*, vol. 58, no. 6, pp. 1182–1195, 2007.
- [20] S. Ravishanker and Y. Bresler, "MR image reconstruction from highly undersampled k-space data by dictionary learning," *IEEE Trans. Med. Imag.*, vol. 30, no. 5, pp. 1028–1041, 2011.
- [21] A. Xenaki, P. Gerstoft, and K. Mosegaard, "Compressive beamforming," *J. Acoust. Soc. Am.*, vol. 136, no. 1, pp. 260–271, 2006.
- [22] P. Gerstoft, C. Mecklenbräuker, A. Xenaki, and S. Nannuru, "Multisnapshot sparse Bayesian learning for DOA," *IEEE Sig. Proc. Lett.*, vol. 23, no. 10, pp. 1469–1473, 2016.
- [23] K. Gemba, S. Nannuru, P. Gerstoft, and W. Hodgkiss, "Multi-frequency sparse Bayesian learning for robust matched field processing," *J. Acoust. Soc. Am.*, vol. 141, no. 5, pp. 3411–3420, 2017.
- [24] T. Wang and W. Xu, "Sparsity-based approach for ocean acoustic tomography using learned dictionaries," *OCEANS 2016 Shanghai IEEE*, pp. 1–6, 2016.
- [25] M. Bianco and P. Gerstoft, "Compressive acoustic sound speed profile estimation," *J. Acoust. Soc. Am.*, vol. 139, no. 3, pp. EL90–EL94, 2016.
- [26] —, "Dictionary learning of sound speed profiles," *IEEE Conf. Acoust., Speech and Sig. Proc. (ICASSP)*, vol. 141, no. 3, pp. 1749–1758, 2017.
- [27] —, "Regularization of geophysical inversion using dictionary learning," *IEEE International Conference on Acoustics, Speech and Signal Processing (ICASSP)*, 2017.
- [28] S. Beckouche and J. Ma, "Simultaneous dictionary learning and denoising for seismic data," *Geophys.*, vol. 79, no. 3, pp. 27–31, 2014.
- [29] Y. Chen, "Fast dictionary learning for noise attenuation of multidimensional seismic data," *Geo. J. Int.*, vol. 209, no. 1, pp. 21–31, 2017.
- [30] M. Taroudakis and C. Smaragdakis, "De-noising procedures for inverting underwater acoustic signals in applications of acoustical oceanography," *EuroNoise 2015 Maastricht*, pp. 1393–1398, 2015.
- [31] L. Zhu, E. Liu, and J. McClellan, "Sparse-promoting full waveform inversion based on online orthonormal dictionary learning," *Geophys.*, vol. 82, no. 2, pp. R87–R107, 2017.
- [32] Y. Huang, M. Ng, and Y. Wen, "A new total variation method for multiplicative noise removal," *SIAM J. Im. Sci.*, no. 2, pp. 20–40, 2009.
- [33] A. Hyvärinen, J. Hurri, and P. Hoyer, *Natural Image Statistics: A Probabilistic Approach to Early Computational Vision*. Springer Sci. Bus. Media, 2009.
- [34] I. Fedorov, B. Rao, and T. Nguyen, "Multimodal sparse bayesian dictionary learning applied to multimodal data classification," *IEEE Conf. Acoust., Speech and Sig. Proc. (ICASSP)*, pp. 2237–2241, 2017.
- [35] M. Saunders, "Solution of sparse rectangular systems using LSQR and CRAIG," *BIT Num. Math.*, vol. 35, no. 4, 1995.
- [36] Y. Pati, R. Rezaifar, and P. S. Krishnaprasad, "Orthogonal matching pursuit: Recursive function approximation with applications to wavelet decomposition," *27th Annual Asilomar Conference on Signals, Systems and Computers, IEEE Proc.*, pp. 40–44, 1993.
- [37] C. Rodgers, *Inverse methods for atmospheric sounding: theory and practice*. World Sci. Pub. Co., 2000.
- [38] T. Bodin, M. Sambridge, and K. Gallagher, "A self-parametrizing partition model approach to tomographic inverse problems," *Inv. Prob.*, vol. 25, no. 5, 2009.

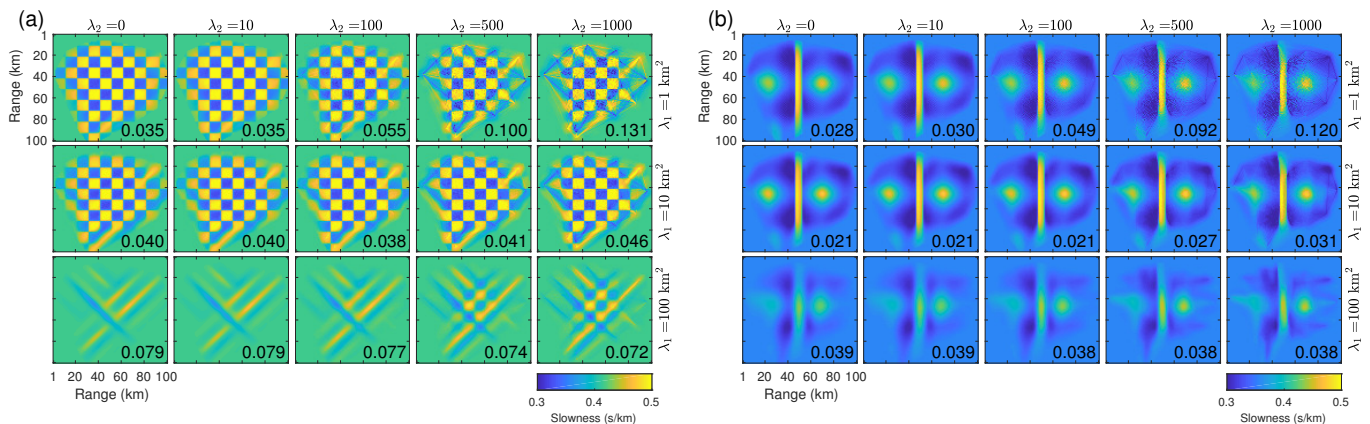


Fig. 12. LST mean $\hat{\mathbf{s}}'_s$ for 100 realizations of Gaussian travel time error with STD of 2% mean travel time, for different values of regularization parameters λ_1 and λ_2 with $n = 100$ for (a) checkerboard $Q = 144$, $T = 1$ (Fig. 3(a)) and (b) smooth-discontinuous $Q = 100$, $T = 2$ (Fig. 3(b)) maps.

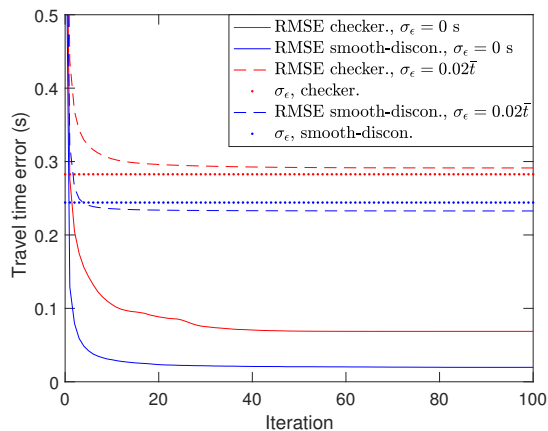


Fig. 13. Travel time RMSE vs. iteration for LST algorithm (Table I) with dictionary learning. Results shown with and without travel time error, corresponding Fig. 5(g,h), 9(g–i) for checkerboard and Fig. 6(j–l), 9(c–h) for smooth-discontinuous slowness maps.

- [39] C. Verlinden, J. Sarkar, W. Hodgkiss, W. Kuperman, and K. Sabra, "Passive acoustic source localization using sources of opportunity," *J. Acoust. Soc. Am. Expr. Let.*, vol. 138, no. 1, pp. EL54–EL59, 2015.
- [40] P. Annibale, J. Filos, P. Naylor, and R. Rabenstein, "TDOA-based speed of sound estimation for air temperature and room geometry inference," *IEEE Trans. Audio, Speech, and Lang. Process.*, vol. 21, no. 2, pp. 234–246, 2013.
- [41] R. Rabenstein and P. Annibale, "Acoustic source localization under variable speed of sound conditions," *Wirel. Comm. Mob. Comp.*, 2017.